Biosensors and Bioelectronics 311 (2026) 118963

Contents lists available at ScienceDirect

Biosensors and Bioelectronics

journal homepage: www.elsevier.com/locate/bios

Experimentally validated dual-band GHz metamaterial perfect absorber biosensor with negative-index response and AI-assisted electromagnetic analysis for breast cancer dielectric discrimination

Musa N. Hamza [a,*], Mohammad Tariqul Islam [b,c,**], Slawomir Koziel [d,e], Mohammad Alibakhshikenari [f,g,***], Bal Virdee [h], Dion Mariyanayagam [h], Sunil Lavadiya [i], Iftikhar ud Din [j], Bruno Sanches [k], Syeda Iffat Naqvi [l], Abinash Panda [m], Ali Farmani [n], Zinelabiddine Mezache [o], Zaid Ahmed Shamsan [p], Homa Farmani [q], Mahdi Ghafourivayghan [r], Muhammad Akmal Chaudhary [s], Mohammad Naser-Moghadasi [t], Md Shabiul Islam [u,v,****]

[a] Department of Physics, College of Science, University of Raparin, Sulaymaniyah, 46012, Iraq
[b] Department of Electrical, Electronic and Systems Engineering, Faculty of Engineering and Built Environment, Universiti Kebangsaan Malaysia, UKM Bangi, Selangor, 43600, Malaysia
[c] Computer and Information Sciences Research Center (CISRC), Imam Mohammad Ibn Saud Islamic University (IMSIU), Riyadh, Saudi Arabia
[d] Engineering Optimization & Modeling Center, Reykjavik University, 102 Reykjavik, Iceland
[e] Faculty of Electronics, Telecommunications and Informatics, Gdansk University of Technology, Gdansk, 80-233, Poland
[f] Lero, The Research Ireland Centre for Software, College of Science and Engineering, School of Computer Science, University of Galway, Galway, H91 TK33, Ireland
[g] Department of Electrical and Electronics Engineering, Dogus University, Umraniye, Istanbul, 34775, Türkiye
[h] Centre for Communications Technology, London Metropolitan University, London, N7 8DB, UK
[i] Department of Information and Communication Technology, Marwadi University, Rajkot, Gujarat, 360003, India
[j] Telecommunication Engineering Department, University of Engineering and Technology, Mardan, 23200, Pakistan
[k] Department of Electronic Systems Engineering, Escola Politécnica da Universidade de São Paulo, Brazil
[l] Department of Telecommunication Engineering, University of Engineering & Technology Taxila, Pakistan
[m] Department of Electronics and Communication Engineering, CMR Institute of Technology, Bengaluru, 560037, India
[n] Department of Electronics Engineering, Lorestan University, Iran
[o] Institute of Optics and Precision Mechanics, University of Ferhat Abbas Setif 1, Setif, 19000, Algeria
[p] Department of Electrical Engineering, College of Engineering, Imam Mohammad Ibn Saud Islamic University (IMSIU), Riyadh, 13432, Saudi Arabia
[q] Department of Nano, Lorestan University, Iran
[r] Ural Federal University, Yekaterinburg, 620002, Russia
[s] Department of Electrical and Computer Engineering, Ajman University, Ajman, United Arab Emirates
[t] Computer and Electrical Engineering Department, Islamic Azad University, Science and Research Branch, Tehran, 14696 69191, Iran
[u] Centre for Advanced Devices and Systems, Centre of Excellence for Robotics and Sensing Technologies, Multimedia University, Persiaran Multimedia, Cyberjaya, Selangor, 63100, Malaysia
[v] Faculty of Artificial Intelligence and Engineering, Multimedia University, Persiaran Multimedia, Cyberjaya, Selangor, 63100, Malaysia

ARTICLE INFO

Keywords:
Metamaterial absorber
Dual-band GHz biosensor
Microwave biosensing

ABSTRACT

A dual-band GHz metamaterial absorber (MPA) biosensor is presented as a proof-of-concept platform for dielectric-sensitive electromagnetic sensing integrated with AI-assisted broadband spectral analysis. The proposed three-layer copper–FR-4–copper structure exhibits near-unity absorption at 6.0 GHz and 9.1 GHz and demonstrates engineered negative-index behavior, which enhances electromagnetic field confinement and

* Corresponding author.
** Corresponding author. Department of Electrical, Electronic and Systems Engineering, Faculty of Engineering and Built Environment, Universiti Kebangsaan Malaysia, UKM Bangi, 43600, Selangor, Malaysia.
*** Corresponding author. Lero, the Research Ireland Centre for Software, College of Science and Engineering, School of Computer Science, University of Galway, H91 TK33 Galway, Ireland.
**** Corresponding author. Centre for Advanced Devices and Systems, Centre of Excellence for Robotics and Sensing Technologies, Multimedia University, Persiaran Multimedia, 63100, Cyberjaya, Selangor, Malaysia.
E-mail addresses: musa.nuraden@uor.edu.krd (M.N. Hamza), tariqul@ukm.edu.my (M.T. Islam), mohammad.alibakhshikenari@universityofgalway.ie (M. Alibakhshikenari), mo.naser@iau.ac.ir (M. Naser-Moghadasi), shabiul.islam@mmu.edu.my (M.S. Islam).

https://doi.org/10.1016/j.bios.2026.118963
Received 23 April 2026; Received in revised form 24 June 2026; Accepted 25 June 2026
Available online 25 June 2026

Triple-negative metamaterials
AI-Assisted spectral analysis
Dielectric-sensitive sensing

sensitivity to dielectric perturbations. The biosensor was fabricated using standard PCB technology and experimentally validated through free-space microwave measurements, showing excellent agreement with simulations and absorption exceeding 92.5% and 99.8% at the two resonant frequencies. For dielectric-sensitive analysis, the sensor response was evaluated under simulation-based loading conditions using low-loss COC/COP coverslip layers and literature-reported electromagnetic properties representative of healthy-like and malignant-like breast environments. Distinct broadband spectral perturbations were observed across the 5–10 GHz frequency range, demonstrating sensitivity to dielectric-property variations. Sensor performance was assessed using quality factor, sensitivity, and figure-of-merit metrics. An AI-assisted spectral interpretation framework was developed using distance- and correlation-based analysis of the broadband electromagnetic response. The results demonstrate that the proposed platform combines dual-band high-Q absorption, engineered triple-negative electromagnetic characteristics, and AI-assisted spectral analysis within a unified microwave biosensing framework. No biological samples were evaluated in this study; therefore, the reported results should be interpreted as simulation-based dielectric-loading analyses rather than validated cancer-detection outcomes.

1. Introduction

Cancer remains a major cause of mortality worldwide, with approximately 20 million new cases and 9.7 million deaths reported in 2022 (Cao et al., 2021; Bray et al., 2024; Bizuayehu et al., 2024). Breast cancer is the most frequently diagnosed malignancy, accounting for about 2.3 million new cases and 670,000 deaths (Liao, 2025). Since early diagnosis substantially improves survival outcomes (Zhang et al., 2025; Pashayan and Pharoah, 2020), there is a continuing need for sensitive, rapid, and minimally invasive techniques for cancer analysis and tissue characterization (Wilson and Sule, 2020; Obeagu and Obeagu, 2024).

Conventional diagnostic methods, including mammography, magnetic resonance imaging, positron emission tomography, histopathology, and molecular biomarker analysis (He et al., 2020; Abdul Halim et al., 2021; Ngan et al., 2020; Hassan et al., 2022; Rotili et al., 2020; Gao et al., 2020; Wekking et al., 2023; Shawky et al., 2020; Kumar et al., 2025; Arun et al., 2024; Dubsky et al., 2024), play essential clinical roles but are often costly, time-consuming, invasive, or reliant on centralized facilities. Likewise, liquid biopsy and MCF-7 cell analysis have attracted considerable interest for cancer diagnostics and biosensor development (Ignatiadis et al., 2021; Zhong et al., 2025; Allen, 2024; Ma et al., 2024; Chen et al., 2022; Tóth et al., 2024; Malhao et al., 2022; Malcolm et al., 2025), although they frequently require complex instrumentation and sample preparation.

To address these limitations, biosensor technologies have received increasing attention (Cerdas et al., 2025; Zafar et al., 2025; Mohammadpour-Haratbar et al., 2023; Bhatti and Kaur, 2025; Sharma et al., 2023; Aldhaeebi and Almoneef, 2023; Pourasl et al., 2023; Wu et al., 2023; Shamim et al., 2024; Mellak et al., 2025; Aliouar et al., 2025; Hamza et al., 2024). In particular, microwave- and metamaterial-based biosensors provide label-free, dielectric-sensitive sensing via engineered electromagnetic interactions (Marvi and Jafari, 2023; Khan et al., 2022; Zhang et al., 2023; Cao et al., 2025; Rahman et al., 2022; Wang et al., 2023; Ghodrati and Uniyal, 2025). Strong electromagnetic-field confinement in metamaterial resonators enhances sensitivity to dielectric perturbations, producing measurable changes in resonant characteristics. Previous studies have demonstrated breast cancer-related dielectric analysis using split-ring resonators, complementary resonators, artificial magnetic conductors, and double-negative metamaterials (Mellak et al., 2025; Khatami et al., 2026; Deng et al., 2023; Jabire et al., 2025; Dadouche et al., 2023; Kamani et al., 2024; Hamza et al., 2025). Meanwhile, artificial intelligence has been increasingly applied to spectral interpretation and biomedical sensing applications (Dubey and Sikarwar, 2025; Saeidnia et al., 2025; Alum, 2025; Hammad et al., 2025; Ng et al., 2023; Uwimana et al., 2025; Smith et al., 2002). Motivated by these developments, this work investigates a conceptual AI-assisted broadband spectral interpretation framework based on GHz metamaterial absorber responses.

A dual-band GHz metamaterial perfect absorber biosensor is proposed for dielectric-sensitive breast tissue characterization. The three-layer copper–FR-4–copper structure exhibits near-unity absorption at 6.0 and 9.1 GHz and engineered triple-negative electromagnetic properties that enhance field confinement and sensitivity. Fabricated using standard printed circuit board technology, the biosensor is experimentally validated through free-space vector network analyzer measurements, showing strong agreement with simulations and absorption exceeding 92.5% and 99.8% at the two resonant frequencies. Using literature-reported dielectric properties of healthy-like and malignant-like breast environments, distinct spectral perturbations are observed over the 5–10 GHz range. A conceptual AI-assisted framework is employed to analyze these broadband responses, thereby demonstrating the proposed platform's potential for future microwave biosensing applications.

Although the electromagnetic performance of the fabricated absorber is experimentally validated, the biological sensing analysis is limited to dielectric-property-based numerical modeling using literature-reported parameters. Therefore, the study should be regarded as a proof-of-concept dielectric-sensitive biosensing framework, providing a basis for future validation using cultured cells and tissue-mimicking phantoms.

2. Modeling framework for the unit cell and electromagnetic assessment

This section presents the design and electromagnetic characteristics of the proposed dual-band metamaterial absorber biosensor operating over the 5–10 GHz range. The biosensor is designed to provide strong absorption, high spectral selectivity, and enhanced sensitivity to dielectric perturbations for microwave biosensing applications. Fig. 1 illustrates the evolution of the unit-cell geometry through three configurations used to optimize resonance behavior and impedance matching.

2.1. Biosensor design strategy for dual-band metamaterial architecture

The proposed biosensor comprises a three-layer copper–FR-4–copper structure designed for dual-band resonant absorption. Fig. 1(a) shows the initial partially symmetric split-resonator geometry with the unit cell dimensions of 10.5×10.5 mm^2, while Fig. 1(b) presents a more symmetric design with optimized notches to improve current distribution and electromagnetic coupling. The final configuration in Fig. 1(c) achieves strong dual-band absorption through enhanced impedance matching and electromagnetic field confinement. The final configuration employs a patterned metallic resonator layer separated from a continuous metallic ground plane by an FR-4 dielectric substrate. This structure supports coupled electric and magnetic resonances, enabling near unity absorption at the target frequencies. The optimized geometric and material parameters used in the design are summarized in Table 1.

2.2. Excitation scheme and optimization of the layered configuration

Fig. 1(d) shows the excitation setup and multilayer structure of the proposed metamaterial absorber biosensor. The device operates in the GHz range with dual absorption peaks at approximately 6 and 9 GHz and can be experimentally validated using standard free-space vector network analyzer measurements.

The structure consists of a patterned metallic resonator on an FR-4 substrate backed by a continuous ground plane, which suppresses transmission, so absorption is governed by reflection reduction. The resonator is designed to simultaneously excite electric and magnetic resonances, enabling impedance matching with free space and near-unity absorption.

The incident wave is defined by its electric field E, magnetic field H, and propagation vector k, with incidence angle θ and polarization angle φ. At resonance, strong field confinement occurs within the resonator and substrate, enhancing sensitivity to dielectric perturbations.

Under simulation-based healthy-like and malignant-like dielectric loading conditions, noticeable shifts in resonance and absorption are observed. The proposed biosensor is further coupled with a conceptual AI-assisted framework for broadband spectral interpretation of GHz responses.

Overall, the compact dual-band design, strong field confinement, and compatibility with standard microwave measurements establish a practical proof-of-concept platform for dielectric-sensitive biosensing.

3. Influence of geometric and constituent parameters on absorption characteristics

This section investigates the influence of resonator geometry and constituent electromagnetic parameters on the absorption performance of the proposed dual-band metamaterial biosensor.

3.1. Comparative analysis of alternative design configurations

Fig. 2(a) and (b) compare the absorption responses of the initial reference geometry (Design Variant 1) and the final optimized biosensor configuration (Design Variant 3). Design Variant 1 exhibits a single absorption resonance at approximately 9.1 GHz with absorption exceeding 99%. In contrast, Design Variant 3 introduces an additional resonance near 6.0 GHz while preserving the high absorption at 9.1 GHz, resulting in a dual-band response with absorption exceeding 92% and 99% at the two resonant frequencies.

Absorption is calculated from the scattering parameters using:

$$A = 1 - |S_{11}|^2 - |S_{21}|^2 \quad (1)$$

Because the metallic ground plane suppresses transmission, the absorption simplifies to:

$$A = 1 - |S_{11}|^2 \quad (2)$$

Table 1
Consolidated representation of the finalized geometric and material parameters utilized in the optimized metamaterial biosensor model.

Parameter	Value (mm)	Parameter	Value (mm)
A	4.035	J	5.67
B	4.035	K	3.27
C	2.035	L	6.636
D	1.68	M	10.5
E	3.68	FR-4 thick (T_1)	1.52
F	2.035	Copper (Cu) thick	35 μm
G	1.558	Dielectric loading thickness (T3)	200 μm
H	3	Coverslip thick (T_2)	100 μm
I	9.61		

Compared with conventional single-band metamaterial absorbers (Mellak et al., 2025; Khatami et al., 2026; Kamani et al., 2024), the proposed dual-band architecture provides increased spectral diversity for dielectric-sensitive electromagnetic analysis.

Similar multi-resonant sensing approaches have been reported in microwave and terahertz metamaterial biosensors (Zhang et al., 2023; Cao et al., 2025; Hamza et al., 2025), where multiple resonances improve sensitivity to dielectric perturbations. The dual-band response therefore provides additional spectral features for monitoring dielectric-loading-induced resonance variations.

3.2. Electromagnetic characterization and parameter retrieval

Fig. 2(c and d) shows the reflection and transmission responses of the optimized biosensor, where strong reflection suppression at both resonant frequencies results in near-unity absorption and confirms effective impedance matching. Fig. 2(e and f) presents the retrieved electromagnetic parameters, exhibiting alternating positive and negative regions of effective permittivity, permeability, and refractive index, indicating engineered negative electromagnetic behavior consistent with reported metamaterial absorbers (Shamim et al., 2024; Khan et al., 2022; Zhang et al., 2023; Cao et al., 2025). Simultaneous negative permittivity and permeability enhance field confinement and interaction with the dielectric environment. The retrieved impedance shows the real part approaching unity and the imaginary part tending to zero at resonance, confirming efficient absorption and minimal reflection.

3.3. Optical response and impedance retrieval

The effective refractive index and impedance were retrieved from simulated scattering parameters under normal incidence. Fig. 2(g) shows the complex refractive index, where alternating positive and negative values confirm resonant metamaterial behavior, while the imaginary part indicates strong attenuation and energy dissipation. Fig. 2(h) compares the reflection coefficient and absorption response, where reflection minima align with absorption maxima, confirming

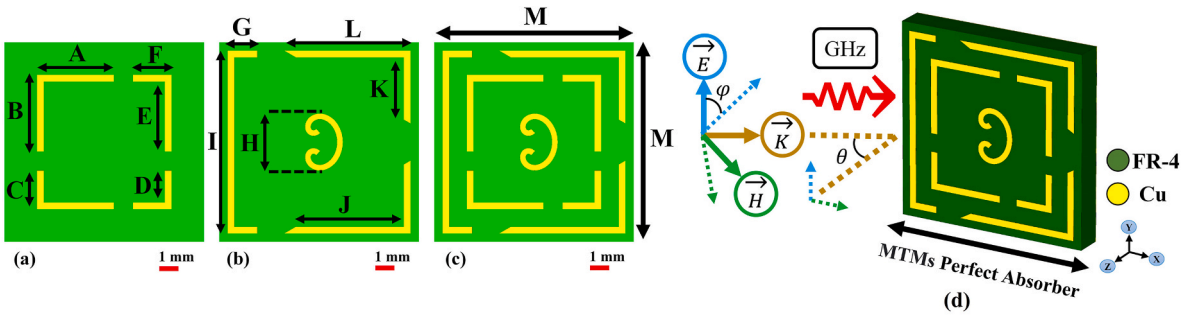

Fig. 1. Conceptual illustration of the proposed metamaterial absorber depicted across three developmental phases: (a) the preliminary structural layout (Design Variant 1), (b) the refined intermediate configuration (Design Variant 2), (c) the fully optimized biosensing geometry (Design Variant 3), (d) schematic illustration of the GHz excitation and multilayer metamaterial absorber biosensor configuration.

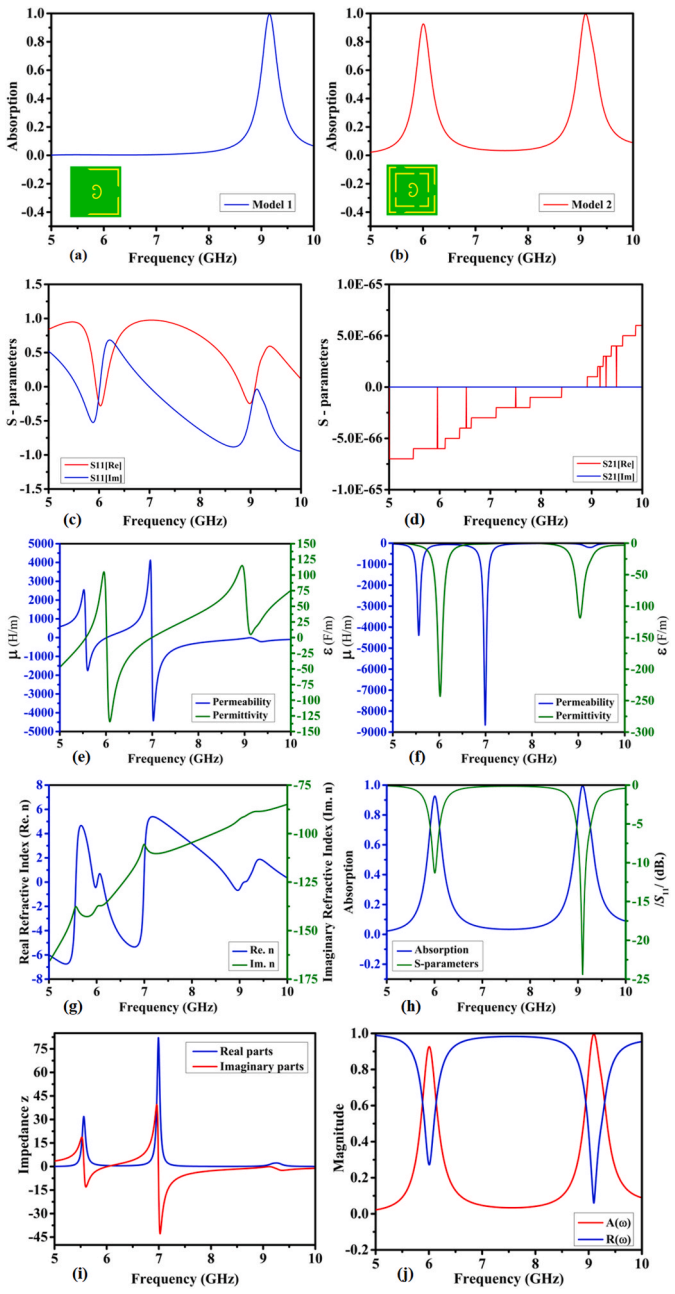

Fig. 2. Simulated electromagnetic performance of the proposed dual-band metamaterial biosensor: (a–b) absorption response evolution from initial (single-band) to optimized (dual-band) design; (c–d) S-parameter (S_{11}, S_{21}) characteristics; (e–f) retrieved effective permittivity (ε) and permeability (μ); (g) refractive index (n); (h) reflection and absorption spectra; (i) effective impedance; and (j) overall reflection–absorption behavior across 5–10 GHz.

impedance matching as the mechanism for high absorption. Fig. 2(i and j) presents the effective impedance, where the real part approaches unity and the imaginary part approaches zero near resonance, indicating excellent free-space matching. Overall, the results confirm strong resonant absorption, negative-index behavior, and enhanced field confinement suitable for dielectric sensing applications.

4. Spatial field profiles and surface current dynamics

This section examines the electric-field, magnetic-field, and surface-current distributions of the proposed dual-band metamaterial absorber at the two resonant frequencies of 6 GHz and 9.1 GHz.

4.1. Electric field distribution

Fig. 3(a–d) shows the electric-field distributions at the two resonant frequencies. At 6 GHz, strong field localization around the spiral resonator and coupling regions confirms excitation of the fundamental mode and effective electromagnetic confinement, with the imaginary component indicating reactive energy storage. Field concentration at split gaps, edges, and coupling regions highlights the dominant interaction sites for dielectric sensing, consistent with reported metamaterial biosensors (Shamim et al., 2024; Zhang et al., 2023; Ghodrati and Uniyal, 2025). This subwavelength energy confinement enhances interaction with the loaded material, improving sensitivity to dielectric changes and enabling spectral discrimination between healthy-like and malignant-like environments. At 9.1 GHz, the field distribution becomes more localized and complex, indicating higher-order mode excitation with stronger coupling, sharper gradients, and enhanced dielectric sensitivity.

4.2. Magnetic field distribution

Fig. 3(e–h) shows the magnetic-field distributions at the two resonances. At 6 GHz, the field is concentrated along resonator edges, indicating magnetic dipole formation and energy trapping via surface currents. At 9.1 GHz, the magnetic field becomes stronger and more distributed, corresponding to higher-order resonances with enhanced confinement and improved dielectric sensitivity under loading.

4.3. Surface current distributions

Fig. 3(i–l) shows the surface-current distributions at 6 and 9.1 GHz. At 6 GHz, currents are mainly concentrated along outer conductive paths, indicating the fundamental mode, while at 9.1 GHz they become more localized and complex, confirming higher-order resonance. Overall, the field and current distributions indicate strong confinement and efficient dual-band resonance, supporting high absorption and dielectric-sensitive sensing capability.

5. Experimental validation

The proposed biosensor was fabricated using standard PCB technology on a 1.52 mm FR-4 substrate with 35 μm copper layers forming the resonator and ground plane. Two prototypes were produced: a 4 × 3 unit-cell sample for fabrication verification and a 21 × 25 array for free-space measurements.

Fig. 4(a–c) shows the fabricated structures and the measurement setup inside an anechoic chamber using a vector network analyzer with a bi-static horn antenna configuration over the 5–10 GHz range. The reflection coefficient S_{11} was measured under normal incidence and used to compute absorption.

Fig. 4(d and e) compares simulated and measured results, showing two resonances near 6 and 9.1 GHz with strong agreement. The fabricated device achieves absorption above 92.5% and 99.8% at the two peaks, confirming near-unity dual-band performance. Minor deviations are attributed to fabrication tolerances, material uncertainty, and alignment errors, but overall agreement validates the design and supports subsequent dielectric-loading analysis.

6. Simulation-based dielectric-sensitive electromagnetic analysis

Following the experimental validation of the fabricated metamaterial absorber, a simulation-based dielectric-loading analysis was conducted to evaluate the sensitivity of the proposed biosensor to variations in electromagnetic properties representative of healthy-like and malignant-like breast environments. The objective of this investigation was to assess the dielectric discrimination capability of the sensor under

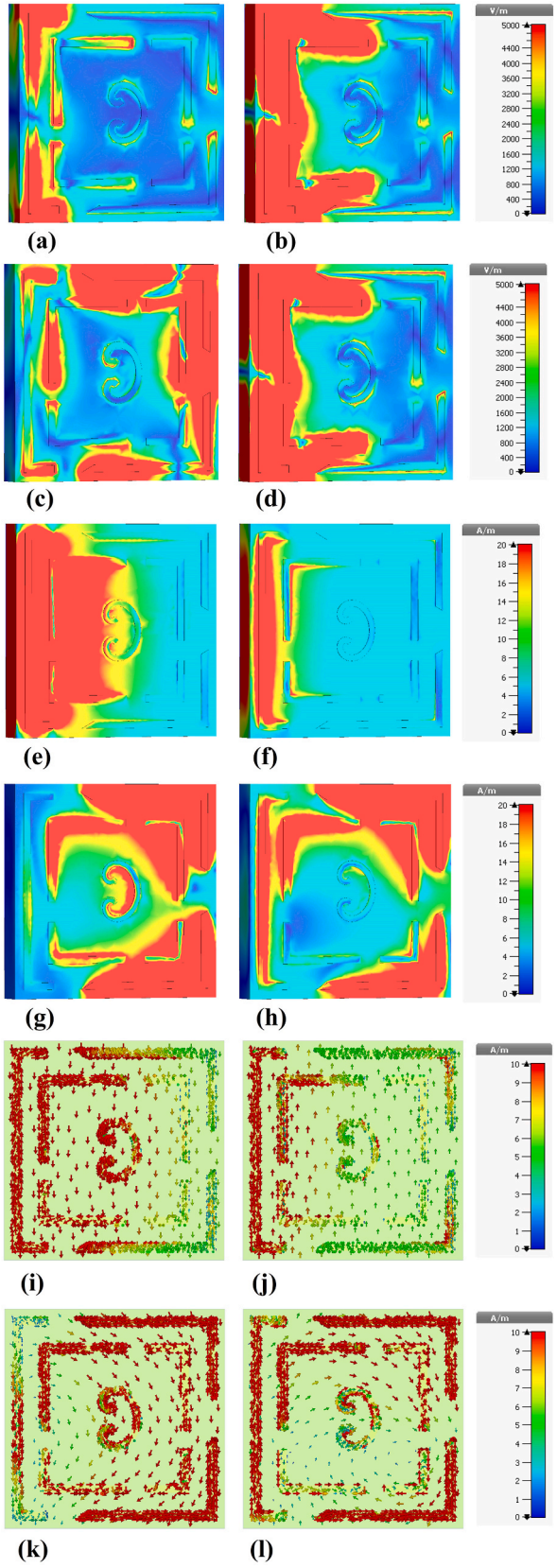

Fig. 3. Electric-field, magnetic-field, and surface-current distributions of the proposed dual-band metamaterial absorber at resonant frequencies: (a–d) electric field |E| at 6.0 and 9.1 GHz; (e–h) magnetic field |H| at 6.0 and 9.1 GHz; and (i–l) surface-current density at 6.0 and 9.1 GHz (real and imaginary components).

controlled electromagnetic conditions rather than to establish clinically validated cancer detection performance. Consequently, no biological samples, cultured cells, tissue phantoms, or ex vivo tissues were utilized in this study.

Fig. 5(a) illustrates the conceptual biosensing configuration employed in the simulations. The structure consists of the experimentally validated metamaterial absorber, a low-loss cyclic olefin copolymer/cyclic olefin polymer (COC/COP) protective layer, and a homogenized dielectric analyte region. The COC/COP layer was selected due to its low dielectric loss, low moisture absorption, and minimal influence on the resonant characteristics of the sensor. The dielectric analyte region was assigned literature-reported electromagnetic properties representative of healthy-like and malignant-like breast dielectric environments (Hussein et al., 2019; Lazebnik et al., 2007; AlSawaftah et al., 2022).

The corresponding absorption responses are presented in Fig. 5(b and c). Distinct spectral variations are observed throughout the 5–10 GHz frequency range, with the malignant-like dielectric environment producing stronger perturbations in both resonance characteristics and broadband spectral behavior. These results demonstrate the sensitivity of the proposed dual-band absorber to dielectric-property variations and confirm its suitability as a dielectric-sensitive electromagnetic sensing platform.

To further investigate broadband spectral discrimination, the complete absorption response was analyzed using an AI-assisted spectral interpretation framework. Rather than relying solely on resonance-frequency shifts, the full spectral response was treated as a multidimensional feature vector. As shown in Fig. 6(b–e), the broadband spectra were transformed into computational feature representations that highlight frequency regions exhibiting the greatest dielectric sensitivity and spectral separability. The strongest discriminative features were concentrated around the dual-resonance regions, indicating that both localized resonant effects and broadband spectral variations contribute to dielectric discrimination.

Fig. 6(f and g) presents conceptual examples of centroid-based spectral categorization using Euclidean-distance and mean-squared-error metrics. Although the analysis was performed using homogenized dielectric-loading models rather than biological measurements, the results demonstrate that the proposed biosensor generates reproducible broadband spectral signatures that can be exploited for AI-assisted electromagnetic classification.

7. Quantitative broadband spectral evaluation

To quantitatively evaluate the dielectric-sensitive response of the proposed biosensor, broadband spectral metrics were derived from the simulated 5–10 GHz absorption responses under healthy-like and malignant-like dielectric loading conditions. Rather than relying solely on resonance shifts, the analysis considers the full broadband spectral response to assess dielectric-sensitive spectral separability.

Let $A_H(f)$ and $A_C(f)$ denote the broadband absorption spectra associated with healthy-like and malignant-like loading conditions, respectively. Treating the spectra as feature vectors enables broadband comparison across the operational frequency range.

7.1. Quality factor

The resonance quality factor evaluates resonance sharpness and spectral selectivity:

$$Q = f_0 / \Delta f \tag{3}$$

where f_0 is the resonance frequency and Δf is the full width at half-maximum bandwidth. Higher Q-factors indicate sharper resonances and improved sensitivity to dielectric perturbations.

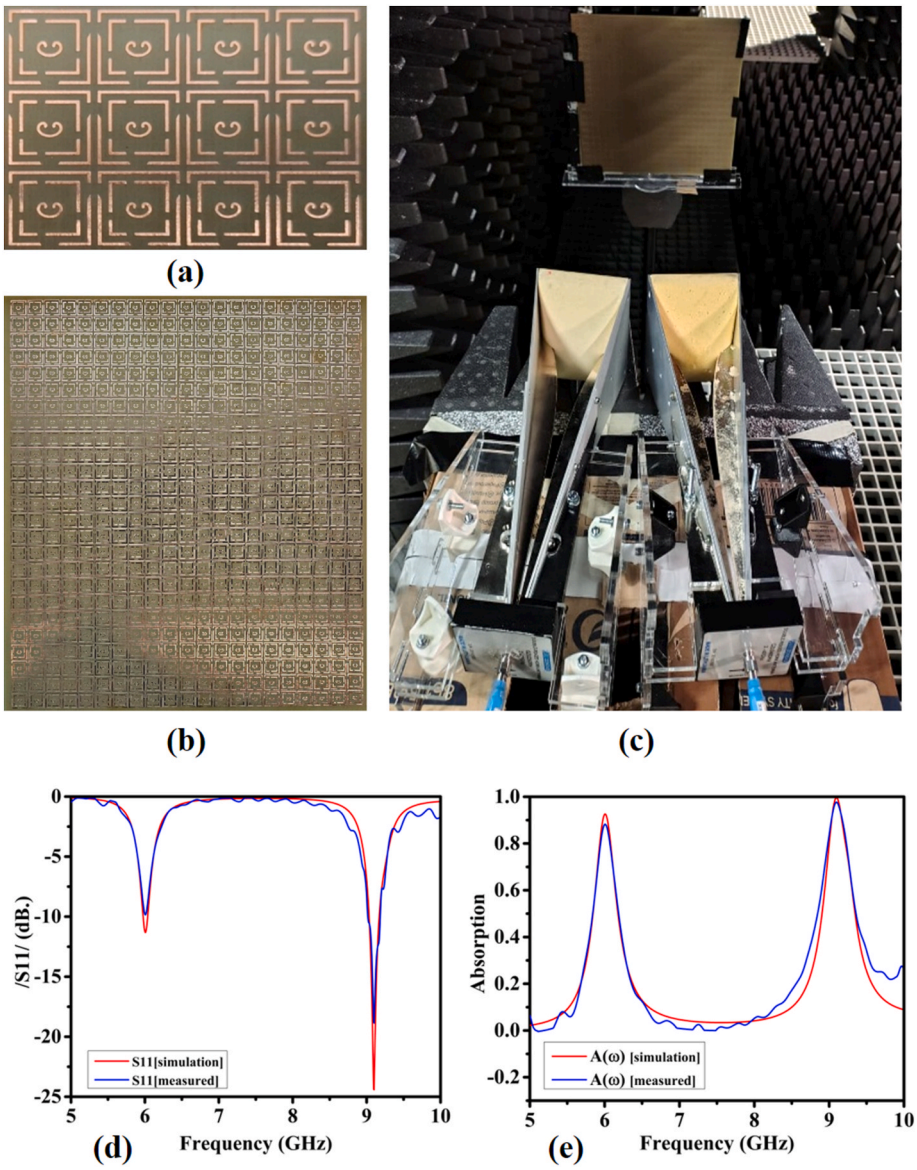

Fig. 4. Fabrication, experimental setup, and electromagnetic validation of the proposed dual-band metamaterial biosensor: (a–b) fabricated unit-cell arrays (4×3 and 21×25 configurations); (c) free-space VNA measurement setup for S_{11} characterization; (d) simulated and measured reflection coefficients (S_{11}); and (e) corresponding simulated and measured absorption spectra confirming dual-band high absorption performance at 6.0 and 9.1 GHz.

7.2. Euclidean sensitivity

Broadband spectral separation between healthy-like and malignant-like responses was quantified using Euclidean sensitivity:

$$S_{EUC} = \sqrt{\sum_{i=1}^{N} (A_C(f_i) - A_H(f_i))^2} \tag{4}$$

Larger values indicate stronger broadband spectral differentiation.

7.3. Area-under-curve sensitivity

The cumulative spectral difference was evaluated using the area-under-curve metric:

$$S_{AUC} = \int \left| A_C(f) - A_H(f) \right| df \tag{5}$$

This metric captures broadband energy variations between the two loading conditions.

7.4. Figure of merit

To relate dielectric-sensitive spectral discrimination to resonance sharpness, the figure of merit was defined as:

$$FOM = \frac{S_{EUC}}{\Delta f} \tag{6}$$

Together, these quantitative metrics provide a broadband spectral foundation for the conceptual AI-assisted spectral interpretation framework presented in the following section.

8. Conceptual AI-assisted broadband spectral interpretation framework

The proposed AI-assisted framework is a proof-of-concept computational approach for broadband spectral interpretation based on simulation-derived electromagnetic responses under controlled dielectric-loading conditions. It is not a clinically validated diagnostic system and does not include experimental biological datasets,

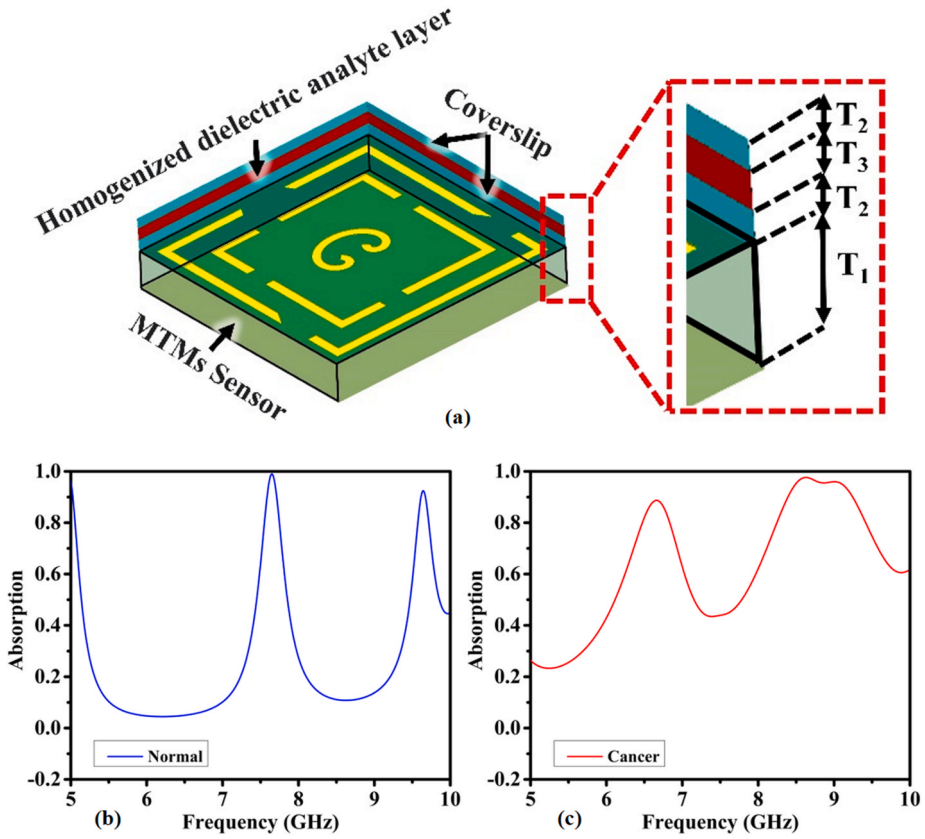

Fig. 5. Simulation-based dielectric-loading analysis: (a) conceptual biosensing architecture incorporating the metamaterial absorber, COC/COP protective layer, and homogenized dielectric analyte region; absorption responses under (b) healthy-like and (c) malignant-like dielectric-loading conditions.

multimodal clinical inputs, or physiological noise effects. The full 5–10 GHz absorption response is represented as a spectral feature vector, which is further transformed into structured two-dimensional feature maps via matrix embedding for computational visualization and similarity analysis. These representations correspond to mathematical spectral embeddings rather than physical tissue images.

Let the sampled broadband response be represented as:

$$A(f) = [a_1, a_2, a_3, \ldots, a_N] \tag{7}$$

The spectral vector was reorganized into a two-dimensional matrix representation according to:

$$F(i,j) = a_{((i-1)K+j)} \tag{8}$$

where $F(i,j)$ denotes the resulting spectral feature map. The broadband electromagnetic responses associated with healthy-like and malignant-like loading conditions were subsequently normalized and analyzed using Euclidean-distance, mean-squared-error, and correlation-based similarity metrics.

To quantify spectral perturbations, feature vectors derived from the simulated S_{11} and S_{21} responses were compared using pointwise absolute-difference analysis:

$$D = |V_C - V_H| \tag{9}$$

where V_H and V_C represent the normalized healthy-like and malignant-like spectral feature vectors, respectively. The resulting broadband spectral differences were used for conceptual centroid-based categorization using threshold-based similarity analysis.

Fig. 7(a) illustrates spectral separability between healthy-like and malignant-like dielectric-loading conditions using an AI-assisted framework. Unlike conventional resonance-tracking methods, the approach utilizes the full 5–10 GHz broadband electromagnetic response for enhanced dielectric-sensitive interpretation. The analysis is based solely on simulation-derived datasets under controlled conditions and does not incorporate biological heterogeneity, tissue morphology, or physiological electromagnetic noise effects.

9. Conceptual spectral decision framework

This section presents a conceptual AI-assisted spectral comparison methodology for broadband interpretation of simulation-derived GHz electromagnetic responses under healthy-like and malignant-like dielectric-loading conditions. Multiple similarity metrics were employed to compare unknown spectral responses against reference spectra, improving robustness beyond single-metric resonance analysis.

Let $A_U(f)$ denote the absorption spectrum of an unknown sample, while $A_H(f)$ and $A_C(f)$ represent the healthy-like and malignant-like reference spectra, respectively.

9.1. Mean-squared error and euclidean-distance analysis

The mean-squared error (MSE) was used to quantify spectral mismatch between unknown and reference responses:

$$MSE = \frac{1}{N}\sum_{i=1}^{N}(A_U(f_i) - A_R(f_i))^2 \tag{10}$$

where $A_R(f)$ denotes the corresponding reference spectrum.

Broadband geometric spectral separation was further evaluated using Euclidean distance:

$$D = \sqrt{\sum_{i=1}^{N}(A_U(f_i) - A_R(f_i))^2} \tag{11}$$

Lower MSE and Euclidean-distance values indicate stronger spectral similarity between the unknown and reference responses.

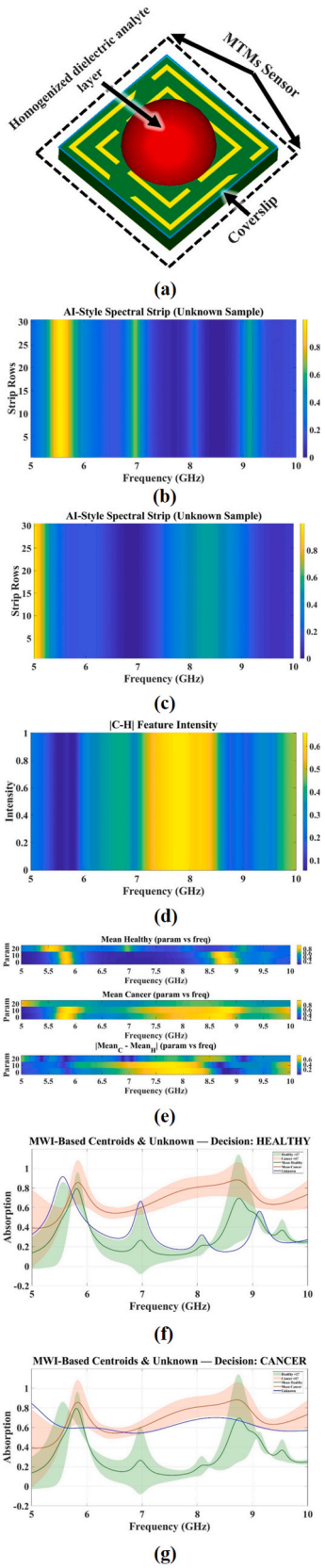

Fig. 6. AI-assisted broadband spectral interpretation: (a) conceptual dielectric-loading model; (b–e) computational spectral feature representations and dielectric-sensitive response maps derived from broadband absorption spectra; (f,g) centroid-based spectral discrimination examples under healthy-like and malignant-like dielectric-loading conditions.

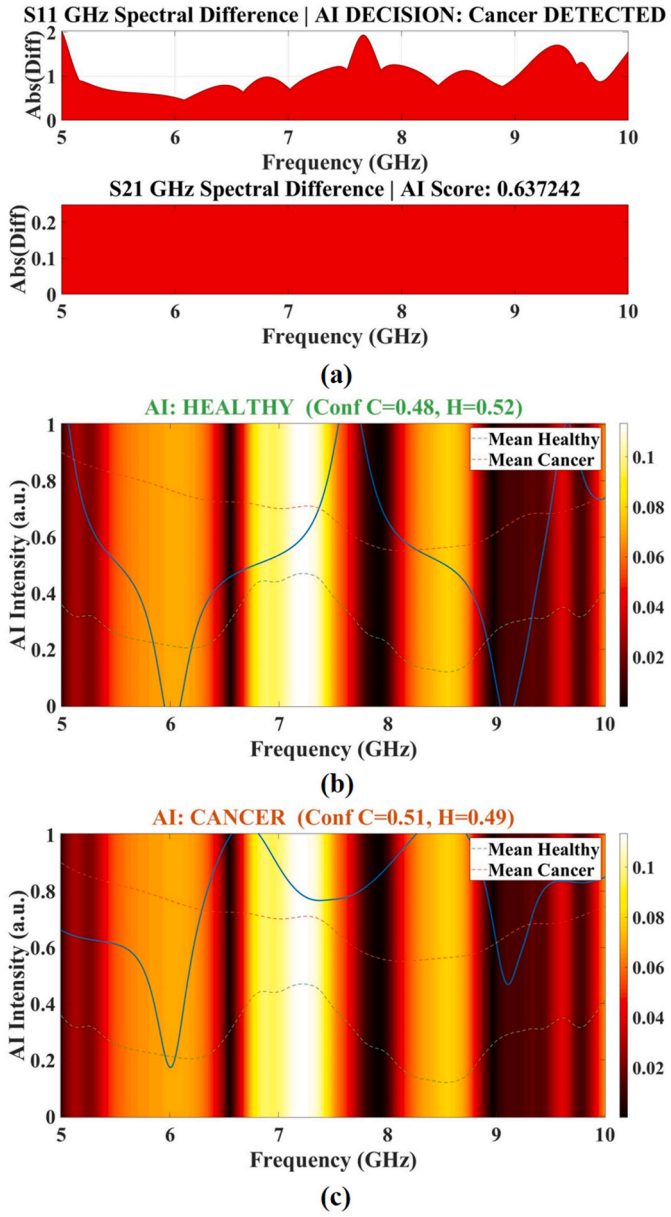

Fig. 7. AI-assisted spectral analysis of simulation-derived GHz responses: (a) feature separability under healthy-like and malignant-like dielectric loading; (b–c) classification outcomes for unknown samples using correlation, MSE, and Euclidean distance metrics.

9.2. *Correlation-based spectral similarity*

To evaluate spectral-shape similarity independent of amplitude variations, Pearson correlation analysis was employed:

$$r = \frac{\sum \left(A_U - \bar{A}\right)\left(A_R - \bar{A}\right)}{\sqrt{\sum \left(A_U - \bar{A}\right)^2 \sum \left(A_R - \bar{A}\right)^2}} \tag{12}$$

Higher correlation values indicate stronger similarity between broadband spectral patterns.

9.3. *Conceptual AI-assisted classification*

The AI-assisted classification framework employs MSE, Euclidean distance, and correlation metrics to assess spectral similarity between

unknown and reference dielectric-loading conditions. As illustrated in Fig. 7(b and c), representative outcomes demonstrate separability between healthy-like and malignant-like responses. The analysis is based solely on simulation-derived electromagnetic data and is therefore considered a proof-of-concept approach. Future work will utilize experimental datasets from phantoms, cultured cells, and ex vivo tissues to evaluate robustness under realistic biosensing conditions.

10. Benchmarking against representative GHz metamaterial perfect absorbers

To assess the significance of the proposed platform, benchmarking was performed against representative GHz-range metamaterial perfect absorbers (MPAs) reported in the recent literature (Mellak et al., 2025; Khatami et al., 2026; Deng et al., 2023; Jabire et al., 2025; Dadouche et al., 2023; Kamani et al., 2024; Hamza et al., 2025; Mohammed et al., 2023; Landy et al., 2008; Kazemi et al., 2025; Yu et al., 2018; Rahman et al., 2024; Wu et al., 2025; NOTO et al., 2025; Rabbani et al., 2024; Li et al., 2025; Ahmed et al., 2025; Han et al., 2025; Rodini et al., 2025; Edries et al., 2023; Liu et al., 2016; Ullah et al., 2024a; Ullah et al., 2024b; Ullah et al., 2024c). The comparison considers electromagnetic performance, structural characteristics, sensing functionality, and spectral-analysis capabilities.

As summarized in Table 2, the proposed biosensor combines experimentally validated dual-band operation with absorption exceeding 92.5% and 99.8% at 6.0 GHz and 9.1 GHz, respectively. The compact copper–FR-4–copper architecture (10.5 mm × 10.5 mm) exhibits engineered triple-negative electromagnetic behavior near resonance, characterized by simultaneous negative effective permittivity, permeability, and refractive index. These characteristics contribute to enhanced electromagnetic field confinement and increased sensitivity to dielectric perturbations. In addition, the device demonstrates a maximum quality factor of 22.61 while maintaining excellent agreement between simulated and measured responses obtained from fabricated PCB prototypes.

Beyond conventional absorber performance, the proposed platform incorporates dielectric-sensitive broadband spectral analysis. Unlike traditional resonance-tracking approaches that primarily utilize isolated resonant-frequency shifts, the present framework exploits the complete 5–10 GHz spectral response under simulation-based dielectric-loading conditions representative of healthy-like and malignant-like breast environments. As summarized in Table 3, broadband spectral evaluation enables the extraction of multiple frequency-domain features associated with dielectric-property variations.

A distinguishing aspect of the proposed approach is the integration of AI-assisted spectral interpretation using distance-based and correlation-based similarity metrics. Rather than functioning solely as a passive electromagnetic absorber, the biosensor combines experimentally validated GHz metamaterial sensing with computational broadband spectral analysis, enabling dielectric-sensitive electromagnetic discrimination within a unified proof-of-concept framework.

Overall, the benchmarking results demonstrate that the proposed platform integrates dual-band high-Q absorption, engineered triple-negative electromagnetic characteristics, broadband dielectric-sensitive spectral analysis, and AI-assisted interpretation within a compact experimentally validated microwave biosensing architecture. These attributes support its potential for future intelligent electromagnetic sensing and microwave imaging applications.

Table 2
Technical and electromagnetic comparison between the proposed biosensor and representative recent GHz metamaterial perfect absorbers (MPAs).

Metric	Proposed biosensor (this work)	Representative recent GHz MPAs
Operating frequencies	Dual-band operation within 5–10 GHz with resonances at 6.0 GHz and 9.1 GHz	Reported designs span single-, dual-, and multi-band microwave absorbers operating approximately from 3 to 40 GHz depending on application requirements (Mohammed et al., 2023).
Absorption magnitude	>92.5% at 6 GHz and >99.8% at 9.1 GHz	Many recent GHz MPAs report near-unity absorption (>90%) at one or multiple resonant frequencies (Landy et al., 2008).
Effective electromagnetic parameters	Engineered simultaneous negative permittivity ($\varepsilon_{eff} < 0$), permeability ($\mu_{eff} < 0$), and refractive index ($n_{eff} < 0$) near resonance regions	Most reported MPAs exploit resonant electric and magnetic responses for impedance matching; explicit triple-negative parameter regions have been comparatively less frequently explored in experimentally validated GHz absorber studies (Kazemi et al., 2025).
Geometry and material stack	Three-layer copper–FR-4–copper configuration; substrate thickness 1.52 mm; unit-cell size 10.5 mm × 10.5 mm	Typical MPAs employ patterned metallic resonators over dielectric substrates backed by continuous metallic ground planes. FR-4 is commonly used in microwave-frequency implementations (Yu et al., 2018).
Resonance quality (Q-factor)	Maximum Q-factor of 22.61 with sharp dual-band resonances	Reported Q-factors vary significantly depending on bandwidth objectives and resonator geometry; many designs prioritize either broadband absorption or narrowband high-Q operation (Rahman et al., 2024).
Validation approach	Experimental electromagnetic validation using fabricated PCB prototypes and free-space VNA measurements; biosensing analysis performed using simulation-based dielectric loading.	Many reported works provide either simulation-only validation or electromagnetic experimental characterization, while relatively fewer studies investigate dielectric-sensitive biological-loading scenarios within experimentally validated GHz absorber platforms (Mellak et al., 2025; Khatami et al., 2026; Deng et al., 2023; Jabire et al., 2025; Dadouche et al., 2023; Kamani et al., 2024; Hamza et al., 2025).

11. Future perspective

Future work will focus on experimental validation using tissue-mimicking phantoms, cultured cell systems, and ex vivo biological samples to evaluate sensing performance under realistic dielectric conditions. Additional research will investigate tunable metamaterial designs, microfluidic integration, and portable microwave sensing platforms. The AI-assisted spectral analysis framework will also be extended using experimentally acquired datasets and advanced machine-learning approaches. Collectively, these developments may facilitate the translation of dielectric-sensitive metamaterial biosensors toward practical microwave diagnostic applications.

12. Limitations and future work

Although the proposed dual-band metamaterial absorber was experimentally fabricated and validated through free-space microwave

Table 3
Functional and practical benchmarking of the proposed biosensor relative to representative recent GHz metamaterial perfect absorbers (MPAs).

Novelty/Practical Metric	Proposed biosensor (this work)	Representative recent GHz MPAs/literature trends
Triple-negative electromagnetic response for dielectric-sensitive biosensing	Simultaneous negative permittivity ($\varepsilon_{eff} < 0$), permeability ($\mu_{eff} < 0$), and refractive index ($n_{eff} < 0$) were engineered near resonance regions to enhance field confinement and strengthen sensitivity to dielectric perturbations under simulation-based biological loading conditions.	Most reported GHz MPAs primarily exploit resonant electric and magnetic responses for impedance matching and absorption enhancement. Explicit use of engineered triple-negative parameter regions for dielectric-sensitive biosensing has been comparatively less frequently explored in experimentally validated GHz absorber studies aimed at biosensing applications (Landy et al., 2008; Li et al., 2025; Ahmed et al., 2025; Han et al., 2025; Rodini et al., 2025)
Biosensor footprint and integration potential	Compact 10.5 mm × 10.5 mm unit-cell geometry implemented using a standard copper–FR-4–copper stack compatible with array-based sensing and potential portable microwave biosensing platforms.	Reported unit-cell dimensions vary significantly depending on frequency range and application objective. Many GHz absorbers are optimized for stealth, EMI shielding, or energy-harvesting applications rather than biosensing-oriented integration (Edries et al., 2023).
Dual-band resonant sensing strategy	Two distinct resonances at 6.0 GHz and 9.1 GHz provide multiple frequency-domain sensing channels and enable broadband spectral comparison under dielectric loading conditions.	While dual-band and multi-band MPAs are widely reported, relatively few studies investigate broadband dielectric-sensitive spectral perturbation analysis for biologically inspired sensing scenarios (Liu et al., 2016).
High absorption and high-Q resonance behavior	Experimentally validated absorption exceeding 92.5% and 99.8% together with a maximum Q-factor of approximately 22.6 enables sharp resonance behavior and strong spectral contrast.	Many reported absorbers prioritize either broadband absorption or narrowband high-Q operation. Simultaneous achievement of strong absorption and relatively sharp resonances is less common in compact GHz absorber implementations (Rahman et al., 2024).
AI-assisted spectral interpretation framework	A conceptual AI-assisted spectral interpretation methodology based on spectral centroids, Euclidean distance, mean-squared error, and correlation analysis was used to evaluate simulation-derived dielectric loading responses corresponding to literature-reported healthy and malignant breast tissue models.	Existing GHz MPA literature rarely integrates absorber responses with physics-guided spectral interpretation methodologies aimed at biosensing-oriented electromagnetic discrimination (Mohammed et al., 2023; Ullah et al., 2024a).
Compatibility with microwave imaging methodologies	The proposed biosensing framework is structured to support future integration with microwave imaging and broadband electromagnetic sensing architectures.	Most reported MPAs focus primarily on electromagnetic absorber performance metrics and are not explicitly structured for integration with broadband microwave imaging and dielectric-sensitive biosensing workflows (Ullah et al., 2024b, 2024c).

measurements, the biosensing investigation was limited to simulation-based dielectric-loading models derived from literature-reported electromagnetic properties representative of healthy-like and malignant-like breast environments. Consequently, the present work should be interpreted as a proof-of-concept dielectric-sensitive electromagnetic biosensing study rather than a clinically validated cancer-detection system.

The dielectric-loading framework employs a homogenized electromagnetic approximation and does not account for biological complexities such as tissue heterogeneity, extracellular matrix interactions, hydration effects, cell attachment, or surrounding physiological media, all of which may influence the electromagnetic response under practical conditions.

Future work will focus on validation using tissue-mimicking phantoms, cultured breast-cancer and healthy control cell lines, and ex vivo tissue samples. Additional studies will investigate microfluidic integration, experimentally acquired biological datasets, and advanced AI-assisted spectral analysis to improve robustness and support future biologically validated dielectric-sensitive microwave biosensing applications.

13. Conclusions

This study presents an experimentally validated dual-band GHz metamaterial perfect absorber biosensor operating in the 5–10 GHz range with resonances at 6.0 GHz and 9.1 GHz. The fabricated copper–FR-4–copper structure (10.5 mm × 10.5 mm) demonstrates near-unity absorption (>92.5% and >99.8%), with excellent agreement between measured and simulated responses, confirming the robustness of the design methodology. The dual-band behavior arises from engineered resonant coupling that yields effective negative-index characteristics (simultaneously negative ε, μ, and n), leading to enhanced electromagnetic field confinement and increased sensitivity to dielectric perturbations.

Simulation-based dielectric-loading analysis, using literature-reported healthy-like and malignant-like breast electromagnetic models, reveals pronounced broadband spectral variations across the 5–10 GHz range, confirming dielectric-sensitive discrimination through frequency-dependent absorption modulation. Performance metrics, including a maximum Q-factor of 22.61, Euclidean sensitivity of 0.415181 GHz/ε_{eff}, and a figure of merit of 1.0311/ε_{eff}, further demonstrate strong spectral selectivity and sensing capability.

A conceptual AI-assisted framework was introduced using distance- and correlation-based metrics for broadband spectral interpretation and preliminary classification of dielectric-loading states.

However, biological validation was not performed, and all results are based on homogenized dielectric models rather than experimental biological samples. Therefore, the work should be interpreted as a proof-of-concept electromagnetic biosensing study. Future work will focus on validation using tissue-mimicking phantoms, cultured MCF-7 cell models, and ex vivo tissues, together with advanced AI-driven spectral

learning and microfluidic integration for practical biosensing applications.

CRediT authorship contribution statement

Musa N. Hamza: Conceptualization, Data curation, Formal analysis, Investigation, Methodology, Resources, Software, Validation, Visualization, Writing – original draft. **Mohammad Tariqul Islam:** Conceptualization, Formal analysis, Investigation, Resources, Software, Validation, Visualization, Writing – original draft, Writing – review & editing. **Slawomir Koziel:** Conceptualization, Data curation, Funding acquisition, Methodology, Resources, Validation, Visualization, Writing – review & editing. **Mohammad Alibakhshikenari:** Conceptualization, Formal analysis, Funding acquisition, Investigation, Methodology, Project administration, Software, Supervision, Validation, Writing – original draft, Writing – review & editing. **Bal Virdee:** Conceptualization, Data curation, Investigation, Resources, Validation, Writing – review & editing. **Dion Mariyanayagam:** Conceptualization, Data curation, Investigation, Resources, Validation, Writing – review & editing. **Sunil Lavadiya:** Data curation, Formal analysis, Investigation, Methodology, Resources, Validation, Visualization, Writing – review & editing. **Iftikhar ud Din:** Conceptualization, Data curation, Formal analysis, Methodology, Resources, Validation, Writing – review & editing. **Bruno Sanches:** Conceptualization, Formal analysis, Investigation, Methodology, Validation, Visualization, Writing – review & editing. **Syeda Iffat Naqvi:** Conceptualization, Data curation, Investigation, Resources, Validation, Visualization, Writing – review & editing. **Abinash Panda:** Conceptualization, Formal analysis, Methodology, Resources, Validation, Visualization, Writing – review & editing. **Ali Farmani:** Conceptualization, Formal analysis, Investigation, Resources, Validation, Visualization, Writing – review & editing. **Zinelabiddine Mezache:** Data curation, Formal analysis, Methodology, Resources, Validation, Writing – review & editing. **Zaid Ahmed Shamsan:** Data curation, Investigation, Software, Validation, Visualization, Writing – review & editing. **Homa Farmani:** Data curation, Software, Validation, Visualization, Writing – review & editing. **Mahdi Ghafourivayghan:** Conceptualization, Funding acquisition, Investigation, Methodology, Resources, Validation, Writing – review & editing. **Muhammad Akmal Chaudhary:** Data curation, Formal analysis, Methodology, Software, Validation, Writing – review & editing. **Mohammad Naser-Moghadasi:** Investigation, Validation, Visualization, Writing – review & editing. **Md Shabiul Islam:** Data curation, Formal analysis, Methodology, Resources, Supervision, Visualization, Writing – review & editing.

Declaration of competing interest

The authors declare that they have no known competing financial interests or personal relationships that could have appeared to influence the work reported in this paper.

Acknowledgements

Co-funded by the European Union. Views and opinions expressed are however those of the author(s) only and do not necessarily reflect those of the European Union or the European Research Executive Agency. Neither the European Union nor the granting authority can be held responsible for them. Besides that, this publication has emanated from research jointly funded by Taighde Éireann - Research Ireland under Grant number 13/RC/2094_2, the European Union's Marie Sklodowska-Curie Actions under grant number 101126578 and was supported in part by University of Galway. The authors gratefully acknowledge the financial support of the University of Doha for Science and Technology under Grant No. KK-2024-005. Additionally, part of this research has been supported by the Icelandic Research Fund (Grant No. 2410297) and the National Science Centre of Poland (Grant No. 2022/47/B/ST7/00072). In addition to above, this work was carried out with the financial support of the Ministry of Science and Higher Education of the Russian Federation (theme № FEUZ-2026-0013).

Data availability

No data was used for the research described in the article.

References

Abdul Halim, A.A., et al., 2021. Existing and emerging breast cancer detection technologies and its challenges: a review. Appl. Sci. 11 (22), 10753.
Ahmed, S., Alam, T., Kirawanich, P., Singh, M.J., Islam, M.T., 2025. Highly sensitive circle enclosed D-pad resonator-based narrowband Metamaterial Absorber for biosensing applications. IEEE Sens. J. 25 (17), 32536–32545.
Aldhaeebi, M.A., Almoneef, T.S., 2023. Dipole array sensor for microwave breast cancer detection. IEEE Access 11, 91375–91384.
Aliouar, T., Djerfaf, F., Bensafieddine, D.e., Bendelala, F., 2025. A new performed metamaterial biosensor for the early detection of cancer cells. Plasmonics 20 (9), 7611–7618.
Allen, T.A., 2024. The role of circulating tumor cells as a liquid biopsy for cancer: advances, biology, technical challenges, and clinical relevance. Cancers 16 (7), 1377.
AlSawaftah, N., El-Abed, S., Dhou, S., Zakaria, A., 2022. Microwave imaging for early breast cancer detection: current state, challenges, and future directions. J. Imag. 8 (5), 123.
Alum, E.U., 2025. AI-driven biomarker discovery: enhancing precision in cancer diagnosis and prognosis. Discov. Oncol. 16 (1), 313.
Arun, B., Couch, F.J., Abraham, J., Tung, N., Fasching, P.A., 2024. BRCA-mutated breast cancer: the unmet need, challenges and therapeutic benefits of genetic testing. Br. J. Cancer 131 (9), 1400–1414.
Bhatti, E., Kaur, P., 2025. Advances in sensor technologies for breast cancer detection: a comprehensive review of imaging and non-imaging approaches. Discover Artf. Intell. 5 (1), 168.
Bizuayehu, H.M., et al., 2024. Global disparities of cancer and its projected burden in 2050. JAMA Netw. Open 7 (11), e2443198.
Bray, F., et al., 2024. Global cancer statistics 2022: GLOBOCAN estimates of incidence and mortality worldwide for 36 cancers in 185 countries. CA Cancer J. Clin. 74 (3), 229–263.
Cao, L., et al., 2025. Terahertz metamaterial sensors: design theory, optimization approach, and advancements in biosensing applications. Adv. Mater. Technol. 10 (9), 2401358.
Cao, W., Chen, H.-D., Yu, Y.-W., Li, N., Chen, W.-Q., 2021. Changing profiles of cancer burden worldwide and in China: a secondary analysis of the global cancer statistics 2020. Chin. Med. J. 134 (7), 783–791.
Cerdas, M.G., et al., 2025. Exploring the evolution of breast cancer imaging: a review of conventional and emerging modalities. Cureus 17 (4).
Chen, G., Liu, W., Yan, B., 2022. Breast cancer MCF-7 cell spheroid culture for drug discovery and development. J. Cancer Ther. 13 (3), 117.
Dadouche, N., et al., 2023. Design and fabrication of a novel corona-shaped metamaterial biosensor for cancer cell detection. Micromachines 14 (11), 2114.
Deng, Y., Zhang, Y., Zhou, M., Wu, B., Zhou, J., 2023. Application of biosensors in detecting breast cancer metastasis. Sensors 23 (21), 8813.
Dubey, S., Sikarwar, S.S., 2025. Applications of AI in cancer Detection—A review of the specific ways in which AI is being used to detect and diagnose various types of cancer. AI in Disease Detection: Advancements and Applications, pp. 147–166.
Dubsky, P., et al., 2024. BRCA genetic testing and counseling in breast cancer: how do we meet our patients' needs? NPJ Breast Cancer 10 (1), 77.
Edries, M., Mohamed, H.A., Ibrahim, A.A., 2023. A dual band 28/38 ghz metamaterial absorber for 5g applications. J. Infrared Millim. Terahertz Waves 44 (11), 898–911.
Gao, Y., Reig, B., Heacock, L., Bennett, D.L., Heller, S.L., Moy, L., 2020. Magnetic resonance imaging in screening of breast cancer. Radiol. Clin. 59 (1), 85.
Ghodrati, M., Uniyal, A., 2025. Exploring metasurface-based biosensor: new frontiers in sensitivity and versatility for biomedical applications. Plasmonics 20 (7), 5589–5608.
Hammad, M., ElAffendi, M., El-Latif, A.A.A., Ateya, A.A., Ali, G., Plawiak, P., 2025. Explainable AI for lung cancer detection via a custom CNN on CT images. Sci. Rep. 15 (1), 12707.
Hamza, M.N., et al., 2025. Precision multi-band Terahertz metamaterial biosensor with targeted spectral selectivity for early detection of MCF-7 breast cancer cells. IEEE Sens. J.
Hamza, M.N., Koziel, S., Pietrenko-Dabrowska, A., 2024. Design and experimental validation of a metamaterial-based sensor for microwave imaging in breast, lung, and brain cancer detection. Sci. Rep. 14 (1), 16177.
Han, W., et al., 2025. Selectable narrow-band anisotropic perfect absorbers based on α-MoO 3 metamaterials for refractive index sensing. IEEE Sens. J.
Hassan, N.M., Hamad, S., Mahar, K., 2022. Mammogram breast cancer CAD systems for mass detection and classification: a review. Multimed. Tool. Appl. 81 (14), 20043–20075.
He, Z., et al., 2020. A review on methods for diagnosis of breast cancer cells and tissues. Cell Prolif. 53 (7), e12822.
Hussein, M., Awwad, F., Jithin, D., El Hasasna, H., Athamneh, K., Iratni, R., 2019. Breast cancer cells exhibits specific dielectric signature in vitro using the open-ended coaxial probe technique from 200 MHz to 13.6 GHz. Sci. Rep. 9 (1), 4681.

Ignatiadis, M., Sledge, G.W., Jeffrey, S.S., 2021. Liquid biopsy enters the clinic—implementation issues and future challenges. Nat. Rev. Clin. Oncol. 18 (5), 297–312.
Jabire, A., et al., 2025. Development of metamaterial-based biosensor for biomedical applications. Niger. J. Technol. Dev. 22 (1), 115–123.
Kamani, T., Patel, S.K., Alsalman, O., Alsaif, F., 2024. Design and optimization of refractive index biosensor for MDA-MB-231 and MCF-7 breast cancer biomarker detection. Phys. Scri. 99 (10), 105541.
Kazemi, N., Kurt, G.K., Baladi, E., 2025. A self-powered microwave sensor using perfect metamaterial absorbers for liquid characterization. IEEE Trans. Microw. Theor. Tech.
Khan, S.A., et al., 2022. Optical sensing by metamaterials and metasurfaces: from physics to biomolecule detection. Adv. Opt. Mater. 10 (18), 2200500.
Khatami, S.A., Rezaei, P., Danaie, M., 2026. Early diagnosis of breast cancer with a highly accurate dual-band graphene-based refractive index sensor. Journal of Advanced Dielectrics, 2550040.
Kumar, S.V., et al., 2025. Fluorodeoxyglucose positron emission tomography–computed tomography (FDG PET-CT) negative orbital metastasis secondary to breast carcinoma: a diagnostic pitfall. Orbit 44 (6), 815–820.
Landy, N.I., Sajuyigbe, S., Mock, J.J., Smith, D.R., Padilla, W.J., 2008. Perfect metamaterial absorber. Phys. Rev. Lett. 100 (20), 207402.
Lazebnik, M., et al., 2007. A large-scale study of the ultrawideband microwave dielectric properties of normal, benign and malignant breast tissues obtained from cancer surgeries. Phys. Med. Biol. 52 (20), 6093.
Li, Y., Chen, F., Yang, W., 2025. A multifunctional bidirectional metamaterial perfect absorber for efficient narrowband and broadband absorption. Opt. Commun., 131878
Liao, L., 2025. Inequality in breast cancer: global statistics from 2022 to 2050. Breast 79, 103851.
Liu, X., Lan, C., Li, B., Zhao, Q., Zhou, J., 2016. Dual band metamaterial perfect absorber based on artificial dielectric "molecules,". Sci. Rep. 6 (1), 28906.
Ma, L., et al., 2024. Liquid biopsy in cancer: current status, challenges and future prospects. Signal Transduct. Targeted Ther. 9 (1), 336.
Malcolm, J.R., Bridge, K.S., Holding, A.N., Brackenbury, W.J., 2025. Identification of robust RT-qPCR reference genes for studying changes in gene expression in response to hypoxia in breast cancer cell lines. BMC Genom. 26 (1), 59.
Malhao, F., Macedo, A.C., Ramos, A.A., Rocha, E., 2022. Morphometrical, morphological, and immunocytochemical characterization of a tool for cytotoxicity research: 3D cultures of breast cell lines grown in ultra-low attachment plates. Toxics 10 (8), 415.
Marvi, F., Jafari, K., 2023. A biosensing platform based on metamaterials BioNEMS for lab-on-chip systems. IEEE Trans. NanoBioscience 23 (1), 11–17.
Mellak, N., Moulfi, B., Aliouar, T., 2025. A multi-cancer metamaterial biosensor: refractive index-based identification of malignant cells. Opt. Quant. Electron. 57 (9), 523.
Mohammadpour-Haratbar, A., Boraei, S.B.A., Zare, Y., Rhee, K.Y., Park, S.-J., 2023. Graphene-based electrochemical biosensors for breast cancer detection. Biosensors 13 (1), 80.
Mohammed, S.A., Albadri, R.A.K., Al-Badri, K.S.L., 2023. Simulation of the microwave five-band a perfect metamaterial absorber for the 5G communication. Heliyon 9 (9), e19466.
Ng, A.Y., et al., 2023. Prospective implementation of AI-assisted screen reading to improve early detection of breast cancer. Nat. Med. 29 (12), 3044–3049.
Ngan, T.T., Nguyen, N.T., Van Minh, H., Donnelly, M., O'Neill, C., 2020. Effectiveness of clinical breast examination as a 'stand-alone'screening modality: an overview of systematic reviews. BMC Cancer 20 (1), 1070.
NOTO, F., Sato, S., Onoe, H., Kan, T., 2025. Soil moisture monitoring using sheet-type GHz metamaterial perfect absorber. Mechanical Engineering Journal, pp. 25–101.
Obeagu, E.I., Obeagu, G.U., 2024. Breast cancer: a review of risk factors and diagnosis. Medicine 103 (3), e36905.
Pashayan, N., Pharoah, P.D., 2020. The challenge of early detection in cancer. Science 368 (6491), 589–590.
Pourasl, M.H., Vahedi, A., Tajalli, H., Khalilzadeh, B., Bayat, F., 2023. Liquid crystal-assisted optical biosensor for early-stage diagnosis of mammary glands using HER-2. Sci. Rep. 13 (1), 6847.
Rabbani, M.G., et al., 2024. Dumbbell shaped structure loaded modified circular ring resonator based perfect metamaterial absorber for S, X and Ku band microwave sensing applications. Sci. Rep. 14 (1), 5588.
Rahman, A.A.M., et al., 2024. Resonator-based near perfect metamaterial absorber with high EMI shielding for Wi-Fi and 5G applications. Int. J. Optomechatron. 18 (1), 2375497.
Rahman, B.A., et al., 2022. Optical fiber, nanomaterial, and thz-metasurface-mediated nano-biosensors: a review. Biosensors 12 (1), 42.
Rodini, S., Vena, A., Chehade, G., Genovesi, S., Manara, G., Costa, F., 2025. Wireless detection of pressure by using PDMS metamaterial absorber. IEEE Sens. J.
Rotili, A., et al., 2020. Double reading of diffusion-weighted magnetic resonance imaging for breast cancer detection. Breast Cancer Res. Treat. 180 (1), 111–120.
Saeidnia, H.R., Firuzpour, F., Kozak, M., Majd, H.S., 2025. Advancing cancer diagnosis and treatment: integrating image analysis and AI algorithms for enhanced clinical practice. Artif. Intell. Rev. 58 (4), 105.
Shamim, S., Mohsin, A.S., Rahman, M.M., Bhuian, M.B.H., 2024. Recent advances in the metamaterial and metasurface-based biosensor in the gigahertz, terahertz, and optical frequency domains. Heliyon 10 (13), e33272.
Sharma, M.K., Singh, S.P., Badola, P., Kumar, M., Saini, J., Ekuakille, A.L., 2023. Noninvasive microwave-multielement sensor for breast phantoms analysis and tumor detection. IEEE Sens. J. 23 (17), 20207–20214.
Shawky, M., Ali, Z.A.E., Hashem, D.H., Houseni, M., 2020. Role of positron-emission tomography/computed tomography (PET/CT) in breast cancer. Egypt. J. Radiol. Nucl. Med. 51 (1), 125.
Smith, D.R., Schultz, S., Markoš, P., Soukoulis, C.M., 2002. Determination of effective permittivity and permeability of metamaterials from reflection and transmission coefficients. Phys. Rev. B 65 (19), 195104.
Tóth, F., Moftakhar, Z., Sotgia, F., Lisanti, M.P., 2024. In vitro investigation of therapy-induced senescence and senescence escape in breast cancer cells using novel flow cytometry-based methods. Cells 13 (10), 841.
Ullah, N., et al., 2024a. Compact dual-band metamaterial absorber: enhancing electromagnetic energy harvesting with polarization-insensitive and wide-angle capabilities. Opt Laser. Technol. 175, 110829.
Ullah, N., et al., 2024b. Design and experimental validation of a compact dual-band metamaterial perfect absorber for electromagnetic energy harvesting applications. Opt. Mater. 157, 116054.
Ullah, N., Islam, M.S., Hoque, A., Yong, W.H., Soliman, M.S., Islam, M.T., 2024c. A compact-sized four-band metamaterial-based perfect absorber for electromagnetic energy harvesting applications. Opt Laser. Technol. 168, 109836.
Uwimana, A., Gnecco, G., Riccaboni, M., 2025. Artificial intelligence for breast cancer detection and its health technology assessment: a scoping review. Comput. Biol. Med. 184, 109391.
Wang, J., Xu, Z., Kotsifaki, D.G., 2023. Plasmonic and metamaterial biosensors: a game-changer for virus detection. Sens.; Diagnostics 2 (3), 600–619.
Wekking, D., Porcu, M., De Silva, P., Saba, L., Scartozzi, M., Solinas, C., 2023. Breast MRI: clinical indications, recommendations, and future applications in breast cancer diagnosis. Curr. Oncol. Rep. 25 (4), 257–267.
Wilson, J., Sule, A., 2020. Disparity in Early Detection of Breast Cancer.
Wu, L., Yang, L., Cai, B., Cheng, Y., Cheng, Z., 2025. Ultra-broadband plasmonic perfect metamaterial absorber based on all-dielectric triple-vertical-ring nanostructure MXene for full-spectrum solar energy. Phys. B Condens. Matter 708, 417205.
Wu, X., et al., 2023. A D-shaped polymer optical fiber surface plasmon resonance biosensor for breast cancer detection applications. Biosensors 14 (1), 15.
Yu, P., et al., 2018. Metamaterial perfect absorber with unabated size-independent absorption. Opt. Express 26 (16), 20471–20480.
Zafar, S., et al., 2025. Emerging biomarkers for early cancer detection and diagnosis: challenges, innovations, and clinical perspectives. Eur. J. Med. Res. 30 (1), 760.
Zhang, W., et al., 2023. Terahertz metamaterials for biosensing applications: a review. Biosensors 14 (1), 3.
Zhang, Y., et al., 2025. Global burden of female breast cancer: new estimates in 2022, temporal trend and future projections up to 2050 based on the latest release from GLOBOCAN. J. Natl. Cancer Cent. 5 (3), 287–296.
Zhong, H.-J., Zhen, Y., Chen, S., Shi, W., Liang, X., Yang, G.-J., 2025. Advances in CTC and ctDNA detection techniques: opportunities for improving breast cancer care. Breast Cancer Res. 27 (1), 97.